



Investigation of Antennas for a High-Sensitivity Polarization Measurement Sensor

Robert J. Burkholder and Chi-Chih Chen

The Ohio State University

ElectroScience Laboratory

Department of Electrical Engineering
Columbus, Ohio 43212

Final Report 60023151-1
Grant No. N00173-09-1-G031

September 2010

Attn: James J. Genova, Code 5760
Naval Research Laboratory
4555 Overlook Ave., SW
Washington, D.C. 20375-5320

20101013315

REPORT DOCUMENTATION PAGE	1. REPORT NO.	2.	3. Recipient's Accession No.
4. Title and Subtitle Investigation of Antennas for a High-Sensitivity Polarization Measurement Sensor		5. Report Date September 2010	
7. Author(s) Robert J. Burkholder and Chi-Chih Chen		6.	
9. Performing Organization Name and Address The Ohio State University ElectroScience Laboratory 1320 Kinnear Road Columbus, OH 43212		8. Performing Org. Rept. No. 60023151-1	
12. Sponsoring Organization Name and Address Naval Research Laboratory 4555 Overlook Ave., SW Washington, D.C. 20375-5320		10. Project/Task/Work Unit No.	
		11. Contract I or Grant (G) No. 1 (G) N00173-09-1-G031	
		13. Report Type/Period Covered Final Report	
		14.	
15. Supplementary Notes			
16. Abstract (Limit: 200 words) The polarization properties of the electromagnetic fields radiated by a scanning array antenna enclosed within an aerodynamic dielectric radome are analyzed and measured. It is known that the radome causes depolarization effects, and it is of interest to measure the depolarization to a high level of sensitivity. A polarization measurement procedure is developed using a pure linearly polarized reference antenna. A design for this antenna is proposed that is expected to have less than -50 dB cross-polarization in the main beam. The same antenna may be employed as a precision polarization sensor of an arbitrary incoming EM wave.			
17. Document Analysis			
a. Descriptors RADOME DEPOLARI- BEAM CROSS- SLOT ARRAY RADAR ZATION STEERING POLARIZATION ANTENNA ANTENNA			
b. Identifiers/Open-Ended Terms			
c. COSATI Field/Group			
18. Availability Statement Approval for release is required; Distribution is limited.		19. Security Class (This report) Unclassified (ITAR)	21. No. of Pages 26
		20. Security Class (This page) Unclassified	22. Price

Table of Contents

Table of Contents	5
List of Figures	7
Chapter 1 Introduction	9
Chapter 2 Scanning Characteristics of Radiation Through a Radome	11
2.1 Introduction	11
2.1 Frequency Domain Scan Patterns	12
2.2.1 Ideal case with no axial rotation	12
2.2.2 Case with axial rotation	12
2.3 Time Domain Pulse Patterns.....	15
2.4 Higher Order Effects.....	15
2.5 Conclusions.....	16
Chapter 3 Determination of Polarization Rotation from Measurements	18
Chapter 4 Conclusions and Future Work.....	25
References	26

List of Figures

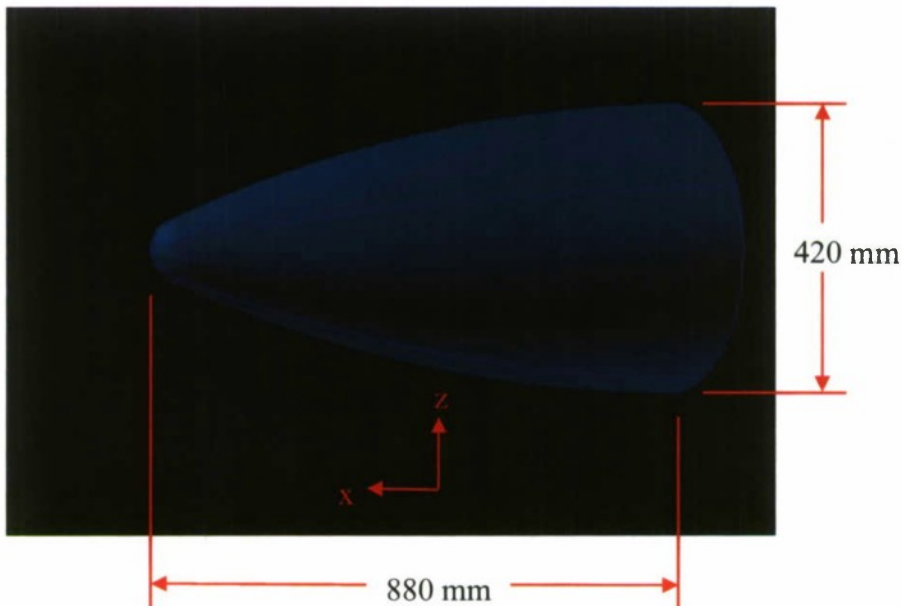
Figure 1.1: Aerodynamic radome geometry rendering from Patran® CAD software.	9
Figure 1.2: Array weighting of circular antenna array in radome.	10
Figure 2.1: Scanning antenna mounted inside a fixed radome with a fixed receiver. The scan direction is \hat{n}_s and the receiver is located at \bar{r} . Azimuth scan angle ϕ_s and receiver angle ϕ_r are shown, although the vectors \hat{n}_s and \bar{r} may have an elevation component as well.....	11
Figure 2.2: Received signal at a fixed receiver as a function of antenna scan angle with no axial rotation of the antenna and radome. Radome is tilted up 3° and the antenna is steered -3° in elevation. Frequency is 9.4 GHz.	13
Figure 2.3: Received signal at a fixed receiver as a function of antenna scan angle with 0.5° axial rotation of the antenna and radome. Radome is tilted up 3° and the antenna is steered -3° in elevation. Frequency is 9.4 GHz.	14
Figure 2.4: Higher order reflection effects from the radome. The green arrows show ray paths that reflect from the radome and the antenna aperture before transmission through the radome.	16

Chapter 1 Introduction

This report finalizes work done under the project “Investigation of Antennas for a High-Sensitivity Polarization Measurement Sensor,” at the Ohio State University ElectroScience Lab (OSU-ESL). Previous work under funding from the Naval Research Laboratory (NRL) investigated the effects of a dielectric nose cone, i.e., aerodynamic radome, on the gain pattern and polarization of an antenna array mounted inside the radome, using numerical, physical optics (PO) and geometrical optics (GO) approaches [1]-[3]. The radome of interest is shown in Figure 1.1, and the circular array enclosed in the radome is shown in Figure 1.2. The array rotates mechanically in elevation and azimuth.

The goals of the present project are:

1. Investigate the scanning characteristics of the antenna array mounted inside the radome as the antenna rotates.
2. Develop a high-precision polarization measurement procedure for accurately characterizing the polarization characteristics of a given antenna.
3. Design a pure linearly polarized reference antenna to be used for measuring the polarization characteristics of an arbitrary antenna, and for use as a polarization sensor.



- The geometry is a body-of-revolution about the x-axis.
- Radome wall is 10 mm thick with relative dielectric 3.315
- Outer radius of tip is 43.9 mm.

Figure 1.1: Aerodynamic radome geometry rendering from Patran® CAD software.

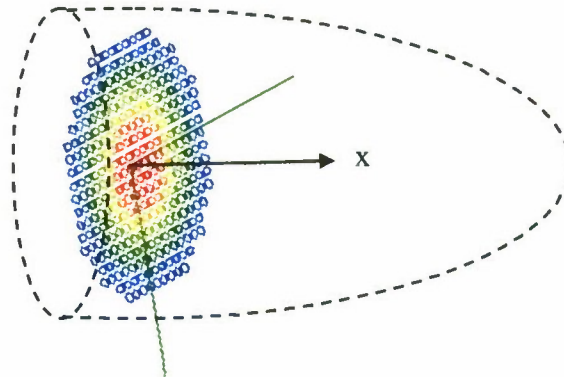


Figure 1.2: Array weighting of circular antenna array in radome.

It was shown in [1] that the radome causes cross-polarized (cross-pol) sidelobes close in to the main beam of the enclosed antenna. The cross-pol was shown to be a result of the different transmission coefficients for two orthogonal polarizations incident on the radome at an oblique angle. Chapter 2 of this report investigates further the cross-pol effect of the radome by examining the received signal at a fixed receiver as the antenna scans in azimuth inside the radome. A method is presented for determining the relative angular offset of the receiver with respect to the radome axis based on the scanning pattern of the enclosed antenna.

Chapter 3 describes a measurement procedure for determining the polarization of an antenna to very high accuracy. It is based on a novel reference antenna design that has a very pure linearly polarized radiation pattern with extremely low cross-pol. An uncertainty analysis is also performed to account for noise and experimental error. The proposed linear antenna may also be employed as a polarization sensor of an arbitrary incoming electromagnetic wave. Hence, Chapter 3 addresses both goals 2 and 3 above.

Conclusions and future work are discussed in Chapter 4.

Chapter 2 Scanning Characteristics of Radiation Through a Radome

2.1 Introduction

In the previous work of [3], the radiation from a circular array antenna enclosed in the radome (see Figure 1.1 Figure 1.2) was computed as a function of angle for a fixed antenna position. Here it is of interest to determine the characteristics of a scanning array by considering the radiated signal at a receiver fixed with respect to the antenna/radome platform, as shown in Figure 2.1. In a realistic situation, the antenna is scanning back and forth in azimuth inside the fixed radome, with scan angle ϕ_s . If we measure the radiated signal at a receiver at \bar{r} as the antenna scans in angle, can we determine the angle ϕ_r , and hence the pointing direction of the radome relative to the receiver direction?

In previous work it was shown that a cross-polarization component is introduced by the radome for certain receiver directions [1]-[3]. This is investigated further here by simulating the received signal at a given receiver location as a function of the antenna scan angle ϕ_s . As will be seen, a complication occurs when the antenna is rotated about the x -axis by an unknown angle. Then it becomes more challenging to use cross-polarization as an indicator of scan angle because the reference co-polarization level is not known. Methods for overcoming this challenge are proposed in the frequency domain and time domain.

In the following, the polarization of the antenna is vertical (z -directed) in the antenna coordinate system. The receiver is in the horizontal azimuth scan plane of the transmitting antenna, and the range to the receiver is 1000m. The radome platform may be tilted slightly in elevation with respect to the scan plane. The numerical results presented here are generated using a modified version of the RADOME code described in [3].

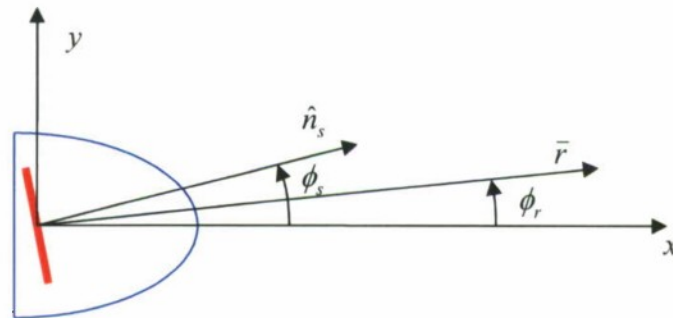


Figure 2.1: Scanning antenna mounted inside a fixed radome with a fixed receiver. The scan direction is \hat{n}_s and the receiver is located at \bar{r} . Azimuth scan angle ϕ_s and receiver angle ϕ_r are shown, although the vectors \hat{n}_s and \bar{r} may have an elevation component as well.

2.1 Frequency Domain Scan Patterns

2.2.1 Ideal case with no axial rotation

Figure 2.2 plots the magnitude and phase patterns of the received signal at a fixed receiver as a function of azimuth scan angle of the antenna in the radome. The radome is tilted up 3° , and the antenna is steered -3° in elevation so that the antenna is scanning in the horizontal plane. Figure 2.2(a) is for a receiver at 0° azimuth, and Figure 2.2(b) is for a receiver at 5° azimuth. Figure 2.2(a) shows that if the radome, antenna, and receiver are all aligned at 0° azimuth, the cross-polarization has a null in the main beam direction, but otherwise it is non-zero. Figure 2.2(b) shows that if the antenna and receiver are aligned at a 5° scan angle, the cross-pol no longer has a null aligned with the main beam. Comparing Figure 2.2(a) and (b), we see that the co-pol pattern is nearly identical in both cases, but the cross-pol pattern null in Figure 2.2(b) is shifted with respect to the co-pol pattern. Therefore, the cross-pol ratio can be used as an indicator of scan angle in this ideal case by measuring the shift in the cross-pol null with respect to the peak in the co-pol scan pattern.

2.2.2 Case with axial rotation

Figure 2.3 plots the same patterns as in Figure 2.2, but with the antenna/radome rotated by 0.5° about the x -axis. As Figure 2.3(a) shows, this small rotation is enough to raise the cross-pol level so that it no longer has a null aligned with the main beam for a receiver in the 0° azimuth direction. The cross-pol ratio is now very similar to the cross-pol ratio of the 5° azimuth case in Figure 2.3(b). Even the phase of the cross-pol ratio is similar. Therefore, the cross-pol ratio can no longer be robustly used as an indicator of the pointing angle. In other words, the main beam scanning patterns look too similar for a receiver at 0° or 5° to determine the actual angle of the receiver relative to the radome. This is true in co-pol, cross-pol, amplitude and phase.

However, if we compare the cross-pol (H-pol) patterns in Figure 2.3 with those of Figure 2.2 we see some significant differences. In Figure 2.2 the null is deeper and the cross-pol pattern is symmetric about the null. Therefore, it may be possible to use the shape of the cross-pol pattern to determine the axial rotation angle. Once this angle is known, the receiver polarization may be counter-rotated to align with the antenna and radome, and then the cross-pol null shift may be ascertained as in Figure 2.2.

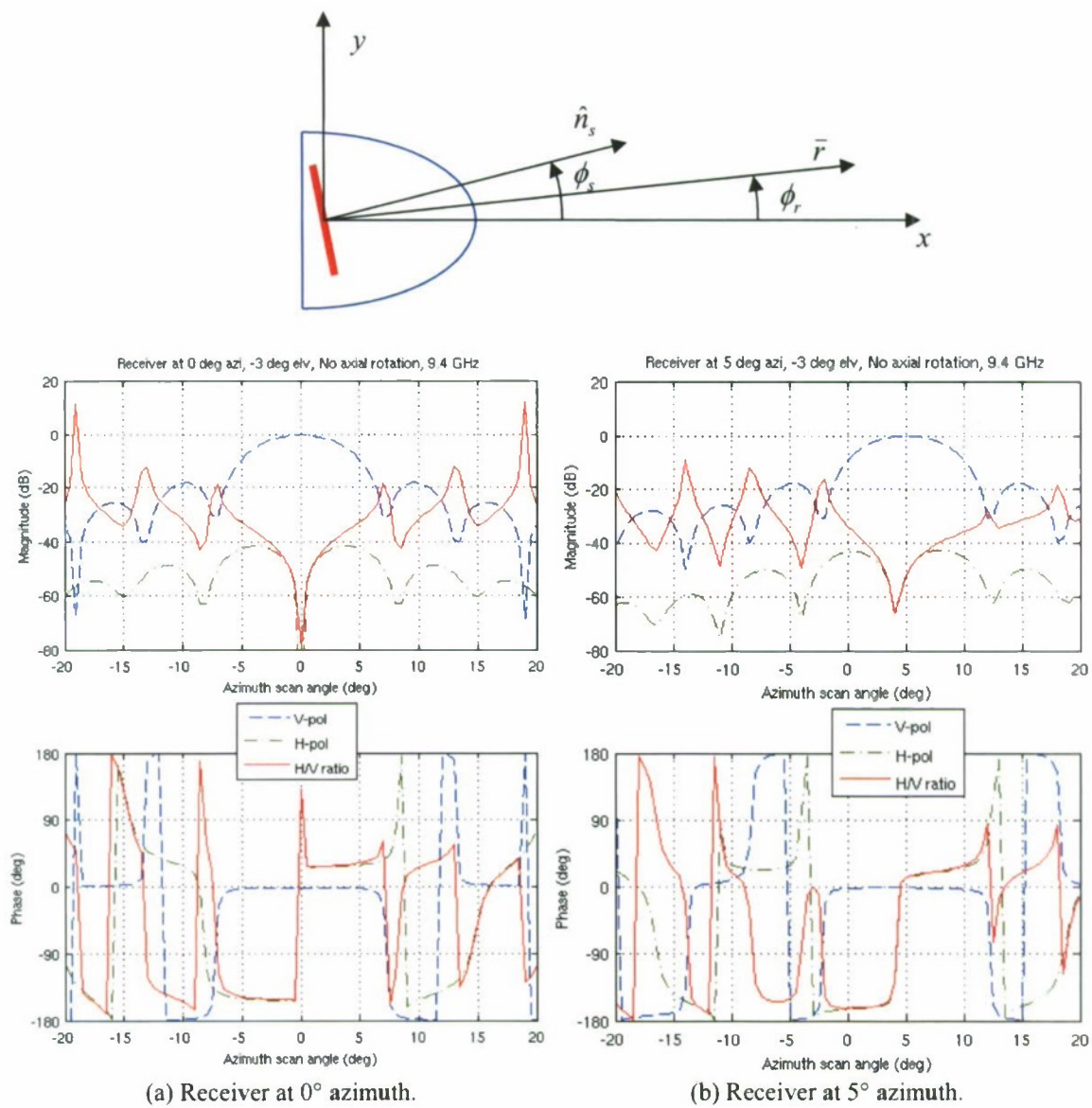


Figure 2.2: Received signal at a fixed receiver as a function of antenna scan angle with no axial rotation of the antenna and radome. Radome is tilted up 3° and the antenna is steered -3° in elevation. Frequency is 9.4 GHz.

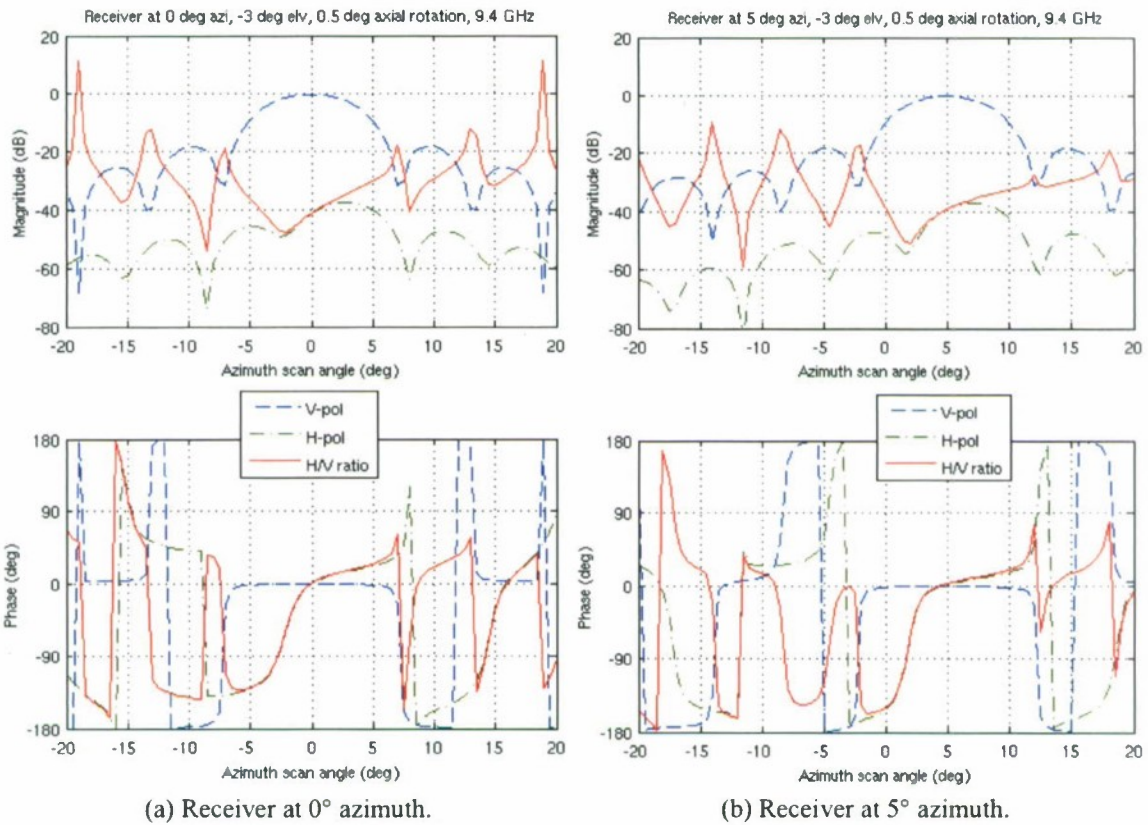
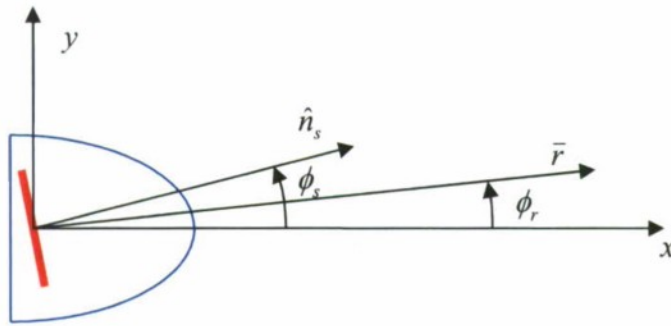


Figure 2.3: Received signal at a fixed receiver as a function of antenna scan angle with 0.5° axial rotation of the antenna and radome. Radome is tilted up 3° and the antenna is steered -3° in elevation. Frequency is 9.4 GHz.

2.3 Time Domain Pulse Patterns

To investigate the effect of the radome on the broadband radar pulses, time domain pulses were obtained by inverse Fourier transform of a 10 MHz radiated signal in the configurations described above. The antenna was scanned in azimuth to point at the receiver, which was at 0° or 5° , with the antenna rotated 0.5° about the x -axis, and not rotated. However, no significant differences in the pulse patterns were observed. This indicates that the first-order frequency variations caused by the radome are not efficacious for determining scan angle.

2.4 Higher Order Effects

The patterns of Figure 2.2 and Figure 2.3 were computed using first-order geometrical optics and physical optics as described in [1]-[3] to include the effect of transmission through the radome. As shown in Section 2.2, this first-order analysis indicates that the received signal is very similar when the receiver is at 0° or 5° azimuth, so it may be very difficult to determine the receiver angle from measurements of the scan pattern. However, there may be significant higher-order effects caused by the radome which have a potential for determining scan angle.

Figure 2.4 shows the dominant ray paths of radiated signals that reflect internally from the radome and then reflect again from the antenna aperture before being transmitted through the radome. In Figure 2.4(a) the antenna is aligned boresight with the radome. In this case there may be strong higher-order interactions that follow ray paths close to the main beam direction. In Figure 2.4(b) the antenna is steered in azimuth with respect to the radome. In this case the reflected rays do not contribute as strongly in the main beam direction because they tend to be deflected more to other angles. It is therefore expected that the higher-order effects of the radome are highly angle dependent. If these effects show up in the scan pattern or time domain pulse patterns, it may be possible to use this information to determine radome pointing direction with respect to the receiver. Detailed numerical studies or measurements are required to quantify this assertion and determine efficacy. There may be other unanticipated higher-order effects that will become apparent from a detailed numerical study and/or measurements as well.

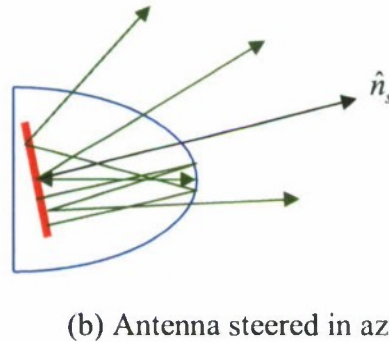
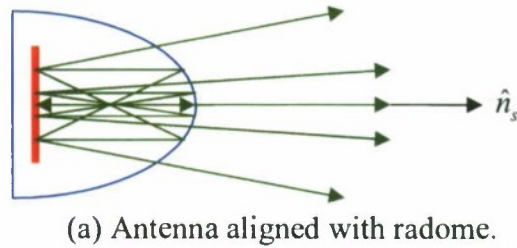


Figure 2.4: Higher order reflection effects from the radome. The green arrows show ray paths that reflect from the radome and the antenna aperture before transmission through the radome.

2.5 Conclusions

First order simulations have indicated that the co-pol and cross-pol scanning patterns of the radome-enclosed antenna may be used to reveal information about the relative orientation of the radome with respect to the receiver direction. If there is no axial rotation of the radome platform and the receiver is located on-axis ($\phi_r = 0$), the cross-pol scan pattern has a null when the antenna is pointed at the receiver ($\phi_s = 0$). A shift in the cross-pol null indicates that the receiver is located away from the radome axis ($\phi_r \neq 0$).

A different situation arises when there is a relative axial rotation of the radome platform with respect to the receiving antenna. In that case a cross-pol component is present simply because of the vector rotation and not necessarily due to the radome effect. The cross-pol scan pattern is very similar when the receiver is on-axis or off-axis, so it may not be possible to determine which is true. However, comparison of the axially rotated and non-rotated scan patterns indicates that the shape of the cross-pol pattern may be used to determine if the radome is rotated or not. It may also be possible to determine the axial rotation angle as follows:

1. Plot the cross-pol pattern at a fixed receiver as the antenna scans in azimuth.
2. Rotate the receiver and re-plot the cross-pol pattern until a symmetric null is formed within the main beam region of the co-pol pattern.

This procedure aligns the receiver with the transmitting antenna. Once aligned, the shift in the null relative to the co-pol main beam direction determines if the receiver is on-axis or off-axis from the radome. Simulations have shown that this should work in theory, but experiments are needed to verify it in real situations.

First-order time domain simulations did not yield any information about scan direction, but there may be hope to use higher order interactions between the radome and antenna array. Detailed numerical simulations and/or measurements are needed to investigate this possibility further.

Chapter 3 Determination of Polarization Rotation from Measurements

The following paper has been submitted to the 2010 Antenna Measurement Techniques Association (AMTA) Conference in Atlanta Georgia, Oct. 10-15. This paper summarizes the work on high-sensitivity polarization measurements supported under the current project. It has been found that the best way to perform such a measurement is with a linearly polarized reference antenna with very low cross-polarization. Such an antenna is proposed using a design that is perfectly symmetric and easy to fabricate. The cross-polarization level is predicted to be less than -50 dB within 5° of the main beam direction, and less than -60 dB within 2° of the main beam direction.

The paper describes the measurement procedure using the reference antenna, and presents an uncertainty analysis based on noise and experimental error. The proposed linearly polarized antenna may also be employed as a polarization sensor of an arbitrary incident electromagnetic wave. Two orthogonally oriented antennas would provide the complete polarization matrix.

A MEASUREMENT TECHNIQUE FOR CHARACTERIZING ANTENNAS WITH LOW CROSS POLARIZATION

Mustafa Kuloglu, Robert J. Burkholder, and Chi-Chih Chen
kuloglu.1@osu.edu, rjb@electroscience.osu.edu, chen.118@osu.edu

ElectroScience Laboratory, Department of Electrical and Computer Engineering
The Ohio State University, 1320 Kinnear Rd.
Columbus, OH 43212

ABSTRACT

This paper discusses a measurement technique for accurately characterizing low cross polarization level of antennas, and associated sensitivity and errors. The technique involves two-antenna transmission (S21) measurement that includes an AUT and a reference antenna that has low cross polarization level. This technique needs two far-field transmission data from two different relative roll angles. The cross-polarization sensitive is determined by SNR of cross-polarization component and cross-polarization of the reference antenna. The cross-polarization error is related to roll angle uncertainty and receiver noise.

Keywords: Antenna Characterization, Antenna Standards, Cross-polarization, RCS Measurements

1. Introduction

Accurately determining the cross-polarization level of an antenna is important in many antenna and radar applications that require accurate polarimetric characteristics. Although measuring co-polarization and cross-polarization gain of an antenna is theoretically straightforward using procedures similar to standard gain measurement procedures. However, the following error sources often limit the sensitivity and accuracy of cross-pol. level with respect to co-pol. component to approximately -40 dB:

- clutter and receiver noise,
- antenna/target orientation uncertainty,
- antenna gain uncertainty,
- lack of antenna standard with accurate calibrated "cross-polarization" level.

"Unintentional" cross-pol. components in an antenna usually arise from fabrication accuracy, design asymmetry, feed leakage, and unbalanced currents. It should be pointed out that even with modern EM

modeling tools, simulating an antenna with perfect geometry symmetry could still yield a cross-polarization level as high as -50 dB due to model meshing unless special care on mesh generation is taken.

One approach to measure an antenna's cross-pol. component is measuring the backscattering radar cross-section (RCS) of a reference target that has known polarimetric scattering characteristics. The RCS of a target is characterized by polarimetric scattering matrix [1-3], has been exploited in many radar calibration methods [4-7]. The calibration procedure used there can be applied polarimetric antenna characterization except that the polarization of the incident from the antenna of interest and unknown. The challenges associated with determining cross-pol. level of an AUT using RCS approach include 1) require accurate scattering matrix associated of the reference target, 2) it is not easy to isolate scattering from target supporting structures, and 3) much weaker signal due to round-trip propagation loss ($1/r^4$), causing poorer cross-pol. sensitivity

Although the standard antenna gain measurement using three-antenna method [8,9] to determine cross-polarization levels of all three antennas involved. The major drawback of this method is the additional errors and uncertainty involved in taking antenna down and mounting antenna up, connecting and disconnecting cables. Such errors and uncertainty severely limits the accuracy low cross-pol. level.

This paper discusses new antenna cross-polarization measurement procedure based on simple AUT-to-REF transmission (S21) measurements by taking advantage of a new ultra-low cross-polarization UWB antenna we recently developed as the reference antenna.

2. Two-Antenna Method for Antenna Cross-Polarization Measurement

Fig.1 illustrates the proposed transmission measurement setup that consists of a reference antenna and an antenna under test (AUT). Both antennas are assumed to be predominantly linearly polarized with low cross-polarization level, and are azimuthally aligned to maximize the S21 response. Assuming that electromagnetic fields are transmitted from the AUT with input power of P_t , the received voltage, V_{rec} , at the reference antenna's port is then expressed as

$$\tilde{V}_{rec} = \sqrt{\frac{2\eta_0 P_t G_{ref} G_{aut} \lambda^2}{(4\pi)^2 r^2}} e^{-jkr} \left[\begin{array}{cc} \sqrt{x_{aut}} \begin{bmatrix} \cos\theta & -\sin\theta \\ \sin\theta & \cos\theta \end{bmatrix} \begin{bmatrix} 1 \\ \sqrt{x_{ref}} \end{bmatrix} \end{array} \right] + N \quad (1)$$

where

- η_0 : free space intrinsic impedance
- P_t : input power
- G_{ref}, G_{aut} : Realized gain for reference antenna and AUT
- λ : wavelength
- r : distance between two antenna at far-field
- x_{aut} : AUT complex cross-pol. level w.r.t. co-pol. of AUT
- x_{ref} : reference antenna complex cross-pol. level w.r.t. co-pol. of reference antenna
- N : receiver noise
- θ : roll angle (see Fig. 1) with $\theta=0^\circ$ defined such that maximum response is observed

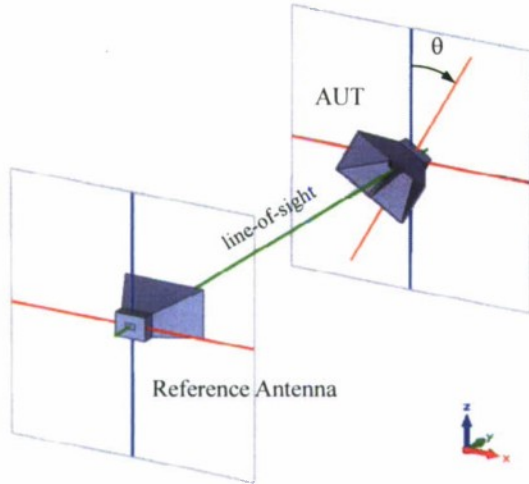


Figure 1 – Two-antenna cross-polarization level measurement setup.

First, the roll position $\theta=0^\circ$ is determined from the maximum response as the AUT rolls over 180 degrees at certain predetermined angle increments (say 0.1 degrees). Note that such $\theta=0^\circ$ position could vary with frequency since the polarization properties of AUT could be function of frequency.

Next, two additional S21 measurements are taken at two different roll angle, i.e. $\theta=\theta_1$ and $\theta=\theta_2$. Using (1), the

received voltages for these two measurements can be expressed as:

$$\tilde{V}_{rec1} = V_{rec1} + N_1 \quad (2a)$$

$$\tilde{V}_{rec2} = V_{rec2} + N_2 \quad (2b)$$

where uncontaminated noise-free received voltage are

$$V_{rec1} = A \left(\cos\theta_1 - \sqrt{x_{ref}} \sin\theta_1 + \sqrt{x_{aut}} \sin\theta_1 + \sqrt{x_{ref}x_{aut}} \cos\theta_1 \right) \quad (3a)$$

$$V_{rec2} = A \left(\cos\theta_2 - \sqrt{x_{ref}} \sin\theta_2 + \sqrt{x_{aut}} \sin\theta_2 + \sqrt{x_{ref}x_{aut}} \cos\theta_2 \right) \quad (3b)$$

$$\text{and } A = \sqrt{\frac{2\eta_0 P_t G_{ref} G_{aut} \lambda^2}{(4\pi)^2 r^2}} e^{j\phi} e^{-jkr}.$$

If we assume that the reference antenna has much lower cross-polarization level than that of the AUT, i.e. $x_{ref} \ll x_{aut}$, taking the ratio of (3a) to (3b) yields

$$\frac{V_{rec1}}{V_{rec2}} \approx \frac{\cos\theta_1 + \sqrt{x_{aut}} \sin\theta_1}{\cos\theta_2 + \sqrt{x_{aut}} \sin\theta_2} \quad (4)$$

Now, the cross-polarization level, x_{aut} can be solve from (4), which gives

$$x_{aut} \approx \left(\frac{V_{rec2} \cos\theta_1 - V_{rec1} \cos\theta_2}{V_{rec1} \sin\theta_2 - V_{rec2} \sin\theta_1} \right)^2 \quad (5)$$

Note that expression in (5) is exact if there is no noise and no cross-polarization component in the reference antenna, i.e. $x_{ref}=0$.

3. Uncertainty Analysis

In reality, measurement data always contains receiver noise, and x_{ref} may not be as low as one would like. This section investigates the error in estimating x_{aut} as a result of noise presence and finite x_{ref} . The estimated cross-polarization level \tilde{x}_{aut} is obtained using the expression in (5) except that actual noise contaminated voltages are used. That is

$$\tilde{x}_{aut} \approx \left(\frac{\tilde{V}_{rec2} \cos\theta_1 - \tilde{V}_{rec1} \cos\theta_2}{\tilde{V}_{rec1} \sin\theta_2 - \tilde{V}_{rec2} \sin\theta_1} \right)^2. \quad (6)$$

The uncertainty definition introduced in [10] was used to define a ‘‘cross-polarization uncertainty’’ (XU) as

$$XU = \frac{\sum_M \left| 10 \log_{10} \left(\frac{|\tilde{x}_{aut}|}{|x_{aut}|} \right) \right|}{M} \quad (7)$$

where M is the number of Monte Carlo simulations. The results shown below were based on $M=40000$ and zero-mean Gaussian noise whose amplitude was chosen to produce a desired signal-to-noise (SNR^{co}) ratio with signal being the maximum co-polarized response (i.e. $\theta_1 = \theta_2 = 0^\circ$). The phase of x_{aut} is modeled as uniformly distributed on $[0, 2\pi]$ radians. The roll angle alignment error is represented by $\Delta\theta$ ($\Delta\theta$ is modeled as a deterministic error).

Cross-Pol. Uncertainty vs. Choice of θ_1 and θ_2

Recall that the proposed method requires two different roll angles. Figure 2 plots XU for different angle combination pairs, while $SNR^{co}=50\text{dB}$, $x_{aut} = -40\text{ dB}$, $\Delta\theta = 0^\circ$, and x_{ref} is held at zero (i.e. $x_{ref}=-\infty\text{ dB}$). It is observed that $\theta_1 \approx -\theta_2$ choice yields lower XU. On the other hand choosing two angles that are close, i.e. near diagonal line, results in high uncertainty values. Our study also showed that this high uncertainty along diagonal increases as noise level increases (or SNR^{co} decreases). It is also observed that choosing a larger angle away from co-pol. direction increases the cross-polarization accuracy. At first glance, this observation may look counter intuitive as the signal power level drops when θ approaches to $\pm 90^\circ$. However, it should be noticed from (4) that within this signal, the contribution coming from x_{aut} is multiplied by $\sin\theta$, which takes greater values as θ approaches to $\pm 90^\circ$.

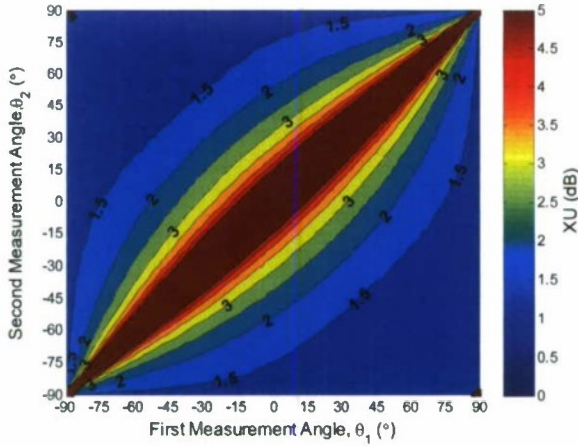


Figure 2 – Cross-pol. uncertainty as a function of measurement angles. ($SNR^{co}=50\text{dB}$, $x_{aut}=-40\text{dB}$, $x_{ref}=-\infty\text{dB}$, $\Delta\theta=0^\circ$)

Cross-Pol. Uncertainty and $\Delta\theta$

Fig. 3 plots the XU results using parameters similar to those used in Fig.2 except that a 0.1° misalignment error for is introduced. This basically means the case when the actual $\theta=0^\circ$ is off by 0.1° . The uncertainty clearly

increases compared the Fig.2 without misalignment error. The minimum uncertainty region with $XU \leq 1.5\text{ dB}$ is near $\theta_1 \approx \theta_2 = 70^\circ$ or $\theta_1 \approx \theta_2 = -70^\circ$.

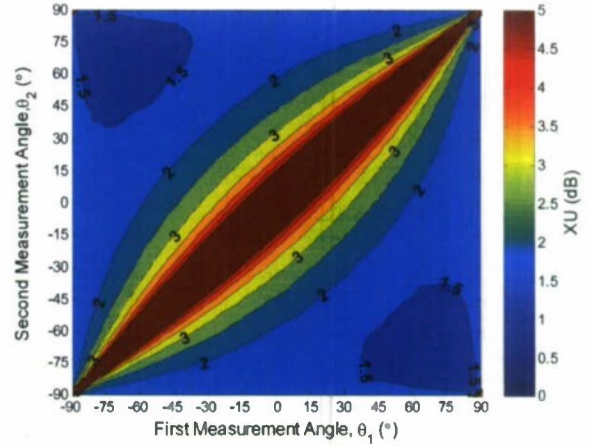


Figure 3 – Cross-pol. uncertainty as a function of measurement angles in the presence of 0.1 degrees angle misalignment. ($SNR^{co}=50\text{dB}$, $x_{aut}=-40\text{dB}$, $x_{ref}=-\infty\text{dB}$, $\Delta\theta=0.1^\circ$)

Cross-Pol. Uncertainty and Reference Antenna Cross-Polarization Level

We will now examine the cross-polarization estimation uncertainty for different noise level (via different SNR^{co}) and reference antenna cross-polarization level (x_{ref}) with the measurement angles fixed at $\theta_1 = -70^\circ$ and $\theta_2 = 70^\circ$. Fig. 4 and Fig. 5 plot resultant XU for $x_{aut} = -40\text{ dB}$ and $x_{aut} = -60\text{ dB}$, respectively. The following observations can be made.

For $x_{aut} = -40\text{dB}$ (Fig.4):

$$XU \leq 3\text{dB} \leftrightarrow SNR^{co} \geq 40\text{dB} \text{ and } x_{ref} \leq -45\text{dB}$$

$$XU \leq 1\text{dB} \leftrightarrow SNR^{co} \geq 50\text{dB} \text{ and } x_{ref} \leq -55\text{dB}$$

For $x_{aut} = -60\text{dB}$ (Fig.5):

$$XU \leq 3\text{dB} \leftrightarrow SNR^{co} \geq 60\text{dB} \text{ and } x_{ref} \leq -65\text{dB}$$

$$XU \leq 1\text{dB} \leftrightarrow SNR^{co} \geq 70\text{dB} \text{ and } x_{ref} \leq -75\text{dB}$$

As a rule of thumb, it can be summarized that in order to be able to measure x_{aut} within 3dB accuracy, SNR^{co} should be bigger than $-(x_{aut}(\text{dB}))$, and x_{ref} should be less than or equal to x_{aut} . That is, the cross-pol. level should be slightly above the noise level and the reference antenna should have a similar cross-polarization level than that of AUT.

Similarly, in order to be able to measure x_{aut} within 1dB accuracy, SNR^{co} should at least 10dB greater than $-(x_{aut}(\text{dB}))$, and x_{ref} should be at least 10dB below x_{aut} . That

is, the cross-pol. level should be 10 dB above the noise level and the reference antenna should have a cross-polarization level 10 dB below than that of AUT.

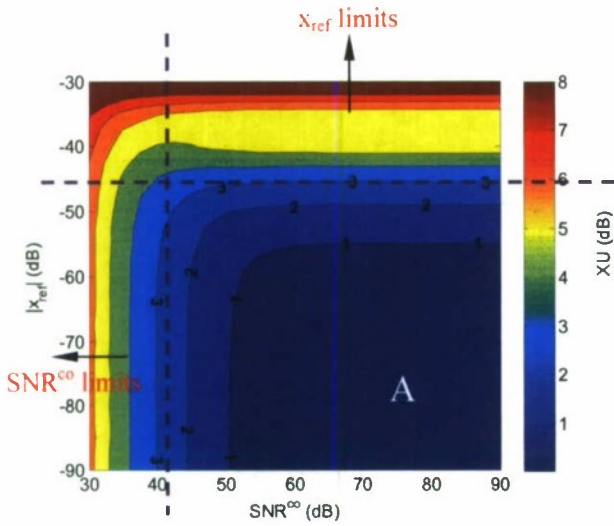


Figure 4 – Cross-pol. uncertainties as a function of SNR^{co} and x_{ref} . ($\theta_1 = -70^\circ$, $\theta_2 = 70^\circ$, $x_{aut} = -40$ dB, $\Delta\theta = 0^\circ$)

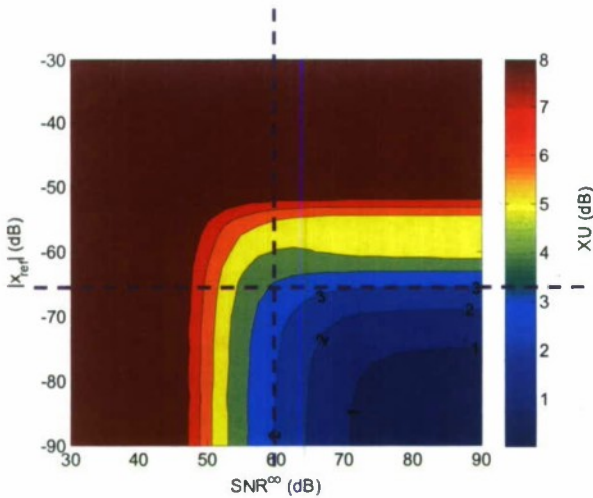


Figure 5 – Cross-polarization prediction uncertainties (XU) as a function of SNR^{co} and x_{ref} . $\theta_1 = -70^\circ$, $\theta_2 = 70^\circ$, $x_{aut} = -60$ dB, $\Delta\theta = 0^\circ$.

4. Ultra-low Cross-Polarization UWB Antenna Design Example

This section discusses about an antenna design example (see Fig.6) that could be used as a standard reference antenna in cross-polarization measurement using procedure proposed in this paper. This design features 3 PCB layers, completely symmetric geometry, and an

external connectorized 0° - 180° hybrid. The bandwidth of this design is expect to achieve 9:1 with cross-polarization level lower than - 50 dB within 5 degrees of main beam and lower than - 60 dB within 2 degrees of main beam. This antenna design is composed of three sections. The first section contains two 50-ohm striplines, each connected to a SMA connector as shown Fig.7(b), which show middle surface with top PCB layer removed for clarity. This section is follow by a 100-ohm slot-line section. Special UWB transition design allowed smooth transition between the two sections. The last section is the tapered-slot antenna section with antenna metallization located on both top and bottom of the thin middle PCB layer (see Fig.6). Notice that the ground plane on the two outer most surface of top and bottom PCB is properly tapered to ensure smooth transition from slot-line to tapered slot antenna.



Figure 6 – Ultra-low cross-polarization tapered slot Antenna with embedded balun network.

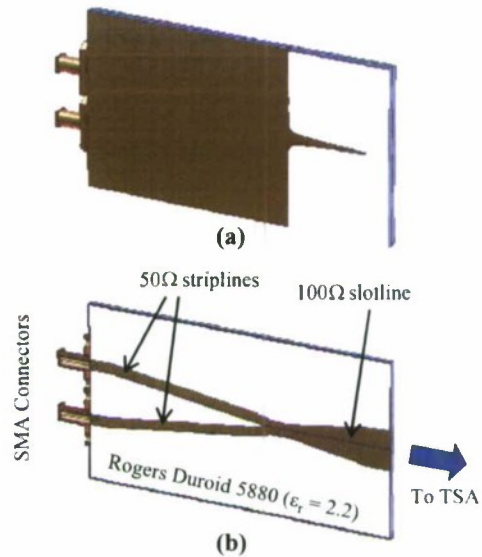


Figure 6 – Feeding network using 180° hybrids. (a) Top and bottom conductor layout, (b) center plane conductor layout. The metallic extension on top and bottom layer improves matching.

Although there are existing designs that utilize various balun design such as coplanar waveguide to slotline, microstrip to slotline, stripline to bilateral slotline transitions [11] for connecting to a coaxial connector. The

residual unbalance component limits the lowest achievable cross-polarization level. To overcome this limitation, we decided to use an external 0° - 180° hybrid to provide two balanced excitations.

A unique SMA connection scheme was developed to ensure physical symmetry and reliable antenna assembling. This is depicted in Figure 7. It consists of three layers of standard Duroid 5880 substrates. The three PCB layers are fabricated and bounded together by PCB manufacturers. A standard edge-mount SMA connector with flat center pin is then slides into the notch created in the middle layer after

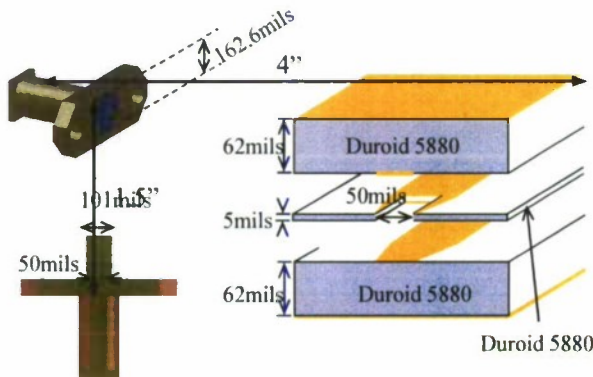


Figure 7 – SMA to stripline connection scheme.

An X-band version of the proposed antenna design was designed and simulated using CST Microwave Studio. The cross-polarization performance of the designed antenna under several unbalance conditions (inherited from the external hybrid) is presented in Figure 9 at 10 GHz. The cross polarization level was found to be less than -50 dB within 5° vicinity of boresight with a balanced hybrid. It was observed that a phase unbalance of 10° in the hybrid cause the minimum cross-polarization location to shift 5 degree in the E-plane. It was found that it can tolerate an amplitude unbalance on 0.5dB without deteriorating the performance.

5. Conclusion

In this paper, a novel measurement method for measuring low level of antenna cross-polarization component was discussed. The theory and formula associated with this method was presented. The results of detail uncertainty analysis were conducted to taking practical measurement uncertainty and receiver noise was also presented. Simple guideline regarding to requirements of noise level and cross-polarization level of the reference antenna were provided as a first order assessment of cross-polarization sensitivity in a given antenna range with a given

reference antenna. A novel ultra-low cross-polarization planar design was also presented. We propose to use such antenna design as an antenna standard for cross-polarization antenna since it should be easy to fabricate and assemble by any PCB manufacturer and users. Unfortunately, we are not able to complete the fabrication and test at the time of this paper submission. However, we expect to present some actual measurement examples during the conference.

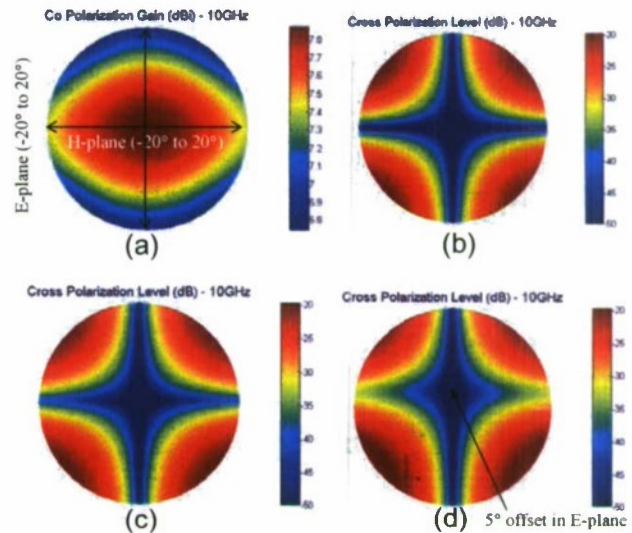


Figure 8 – X-pol performance of the tapered slot antenna. (a) Perfect balance co-pol realized gain, (b) Perfect balance X-pol, (c) 0.5dB amplitude unbalance X-pol, (d) 10-degree phase unbalance X-pol.

6. REFERENCES

- [1] O. Lowenschuss, "Scattering matrix application," *Proceedings of the IEEE*, vol. 53, pp. 988-992, Aug. 1965.
- [2] F. K. Eugene, *Radar Cross Section Measurements*. Scitech Publishing, 2006.
- [3] G. T. Ruck, ed., *Radar Cross Section Handbook*, vol. 1. Plenum Press, 1970.
- [4] J.-R. J. Gau and W. D. Burnside, "New polarimetric calibration technique using a single calibration dihedral," *IEE Proceedings on Microwaves, Antennas and Propagation*, vol. 142, pp. 19-25, Feb. 1995.
- [5] K. Sarabandi, F. T. Ulaby, and M. A. Tassoudji, "Calibration of polarimetric radar systems with good polarization isolation," *IEEE Transactions on Geoscience and Remote Sensing*, vol. 28, pp. 70-75, Jan. 1990.
- [6] K. Sarabandi and F. T. Ulaby, "A convenient technique for polarimetric calibration of single antenna

radar systems," *IEEE Transactions on Geoscience and Remote Sensing*, vol. 28, pp. 1022-1033, Nov. 1990.

[7] M. W. Whitt, F. T. Ulaby, P. Polatin, and V. V. Liepa, "A general polarimetric radar calibration technique," *IEEE Transactions on Antennas and Propagation*, vol. 39, pp. 62-67, Jan. 1991.

[8] A. Newell and D. Kerns, "Determination of both polarisation and power gain of antennas by a generalised 3-antenna measurement method," *Electronics Letters*, vol. 7, pp. 68-70, February 1971.

[9] A. Newell, "Improved polarization measurements using a modified three-antenna technique," *Antennas and Propagation, IEEE Transactions on*, vol. 36, pp. 852-854, Jun 1988.

[10] B. M. Welsh, B. M. Kent, and A. L. Buterbaugh, "Full polarimetric calibration for radar cross-section measurements: performance analysis," *IEEE Transactions on Antennas and Propagation*, vol. 52, pp. 2357-2365, Sept. 2004.

[11] K. F. Lee and W. Chen, *Advances in Microstrip and Printed Antennas*. John Wiley & Sons, 1997

Chapter 4 Conclusions and Future Work

This report has investigated the depolarization effects of a dielectric radome on the radiation pattern of a scanning antenna enclosed inside the radome, and presented a high-precision procedure for measuring polarization and cross-polarization.

As demonstrated in Chapter 2, it is theoretically possible to determine the relative angular offset of the axis of the radome with respect to the receiver direction from a measurement of the scanning pattern of the enclosed antenna. Furthermore, this is possible even if the transmitting and receiving antennas are not perfectly aligned. More detailed simulations and experimental measurements are needed to verify this approach.

Also seen from Chapter 2, first-order time domain simulations did not yield any information about scan direction, but there may be hope to use higher order interactions between the radome and antenna array. Detailed numerical simulations and/or measurements are needed to investigate this possibility further.

The polarization measurement procedure described in Chapter is based on a high-precision linearly polarized reference antenna with extremely low cross-polarization. An antenna design is proposed that is expected to have less than -50 dB cross-polarization in the main beam region. This antenna may be used as a reference antenna for characterizing the polarization properties of existing antennas, or as a high-precision polarization sensor. It remains to fabricate and measure this antenna to verify the design and evaluate its use as a polarization sensor in a realistic application.

References

- [1] R. J. Burkholder and M. Carr, "Radiation Pattern Analysis of an Antenna Enclosed in an Aerodynamic Radome", The Ohio State University ElectroScience Lab, Final Report 60006314-1, Feb. 2006.
- [2] Kezhong Zhao, Robert J. Burkholder, and Jin-Fa Lee, "Radiation Pattern Analysis of an Antenna Enclosed in an Aerodynamic Radome Using a Domain Decomposition Method," The Ohio State University ElectroScience Lab, Final Report 60009498-1, Feb. 2007.
- [3] R. J. Burkholder, "Computer Simulation of a Low-Flying Radar Enclosed in an Aerodynamic Radome," The Ohio State University ElectroScience Lab, Final Report 60009498-2, May 2007.